Journal of Biomolecular NMR, 5 (1995) 122–132
ESCOM

J-Bio NMR 239

The solution structure of ω-Aga-IVB, a P-type calcium channel antagonist from venom of the funnel web spider, *Agelenopsis aperta*

Michael D. Reily[a,*], Venkataraman Thanabal[a] and Michael E. Adams[b]

[a]*Department of Chemistry, Parke-Davis Pharmaceutical Research, Division of Warner Lambert Company, Ann Arbor, MI 48105, U.S.A.*
[b]*Departments of Entomology and Neuroscience, University of California, Riverside, CA 92521, U.S.A.*

Received 29 July 1994
Accepted 27 September 1994

Keywords: Neurotoxic peptide; NMR spectroscopy; Peptide structure; Three-dimensional structure

Summary

The 48 amino acid peptides ω-Aga-IVA and ω-Aga-IVB are the first agents known to specifically block P-type calcium channels in mammalian brain, thus complementing the existing suite of pharmacological tools used for characterizing calcium channels. These peptides provide a new set of probes for studies aimed at elucidating the structural basis underlying the subtype specificity of calcium channel antagonists. We used 288 NMR-derived constraints in a protocol combining distance geometry and molecular dynamics employing the program DGII, followed by energy minimization with Discover to derive the three-dimensional structure of ω-Aga-IVB. The toxin consists of a well-defined core region, comprising seven solvent-shielded residues and a well-defined triple-stranded β-sheet. Four loop regions have average backbone rms deviations between 0.38 and 1.31 Å, two of which are well-defined type-II β-turns. Other structural features include disordered C- and N-termini and several conserved basic amino acids that are clustered on one face of the molecule. The reported structure suggests a possible surface for interaction with the channel. This surface contains amino acids that are identical to those of another known P-type calcium channel antagonist, ω-Aga-IVA, and is rich in basic residues that may have a role in binding to the anionic sites in the extracellular regions of the calcium channel.

Introduction

Peptide toxins from animal venoms are increasingly used as selective and diagnostic probes for functionally distinct types of ion channels in the brain (Olivera et al., 1994) and also hold promise as potent therapeutic agents (Valentino et al., 1993). A common structural motif among peptide toxins is a rigid conformation conferred by multiple internal disulfide bonds. It is noteworthy that, despite the different ion channel specificities of various neurotoxins, the pattern of cysteine placement in their primary structures is relatively constant. For example, members of the ω-agatoxin (Mintz et al., 1992; Adams et al., 1993), ω-conotoxin (Olivera et al., 1994) and μ-agatoxin (Skinner et al., 1989) families share a similar disulfide pattern, but specifically target P-type calcium channels (ω-Aga-IVB), N-type calcium channels (ω-conotoxin GVIA) and sodium channels (μ-agatoxins I–VI), respectively. This raises interesting questions regarding the precise structural features that determine ion channel selectivity. Structural analysis of these toxins by two-dimensional NMR spectroscopy is particularly advantageous because of their high aqueous solubility and rigid character. Information has begun to emerge on the structural properties of several calcium channel-specific toxins, including ω-conotoxin GVIA (Davis et al., 1993; Sevilla et al., 1993), ω-Aga-IVB (Adams et al., 1993; Yu et al., 1993) and ω-Aga-IVA (Reily et al., 1994).

We are interested in determining the precise structural determinants of toxin specificity for P-type calcium channels, which regulate neurotransmitter release and synaptic transmission in the mammalian brain. The 48 amino acid

*To whom correspondence should be addressed.

Abbreviations: TOCSY, total correlated spectroscopy; NOESY, nuclear Overhauser enhancement spectroscopy; COSY, correlated spectroscopy.

Supplementary Material: One page describing details of the structural analysis, one figure showing sequence-specific cross-peak assignments in the fingerprint region of the 80 ms NOESY spectrum and one table containing complete proton resonance assignments.

spider venom toxin, ω-Aga-IVA, was the first high-affinity toxin reported to selectively target these channels (Mintz et al., 1992). More recently, we have described a related toxin, ω-Aga-IVB (Adams et al., 1993), which is conspicuously more abundant in funnel web spider venom. This allowed for the isolation of sufficient quantities of native toxin for the structural determination reported here.*

Materials and Methods

NMR spectroscopy

ω-Aga-IVB was isolated as previously described (Adams et al., 1993). NMR spectra were recorded at 500 or 600 MHz on 4 or 8 mg of peptide dissolved in 0.5 ml of either 10% D_2O/90% H_2O or 100% D_2O at pH 2.6. At this concentration, the peptide became considerably less soluble at pH > 5. All spectra were processed using UXNMR (Bruker). The resulting real portions of the processed data were then transferred to a Silicon Graphics workstation and converted to a FELIX matrix format using the program ux2mat (P. Schmieder, personal communication). TOCSY (Braunschweiler and Ernst, 1983) spectra were acquired with a 60 ms 7 kHz MLEV-17 (Bax and Davis, 1985) spin-lock field. NOESY (Kumar et al., 1980) spectra were acquired with mixing times of 80, 160, 250 or 300 ms with presaturation of the H_2O or HDO signal during the mixing time. Both experiments consisted of either 2048 or 4096 t_2 and 512 or 750 t_1 data points and utilized time-proportional phase incrementation (TPPI) (Marion and Wüthrich, 1983) to achieve phase sensitivity in ω_1. Most experiments were recorded at 15, 25 and 30 °C. Amide protons were characterized as either slowly or very slowly exchanging, based on the presence of corresponding cross peaks in sequentially acquired TOCSY (total acquisition time 2 h) and NOESY spectra (total acquisition time 24–48 h) on samples freshly dissolved in D_2O and recorded at 15 °C. Coupling constants were measured directly from resolution-enhanced 1D spectra recorded in H_2O.

Structure calculations

Well-resolved cross peaks in the NOESY spectra were integrated using FELIX (Biosym Technologies) and were assigned an upper distance bound based on their relative integrated intensity. Poorly resolved cross peaks were classified as strong, medium or weak and corresponding internuclear upper bound distances of 2.5, 3.5 and 5.0 Å, respectively, were assigned to each interaction. Lower bounds were taken to be the sum of the van der Waals radii for the interacting protons in all cases. Backbone ϕ angles were constrained to ranges consistent with measured $^3J_{HN\overline{H}\alpha}$ values and χ^1 angles for several amino acids were constrained based on observed NOE and J coupling patterns (Wagner et al., 1987). In some calculations, hydrogen bonds were introduced by setting a generic distance constraint of 2.35 Å between a selected slowly exchanging NH proton and an acceptor atom. Structures were generated using the NMR-derived restraints as input to a distance geometry/simulated annealing algorithm, DGII (Havel, 1991) using triangle bounds smoothing, a four-dimensional embed algorithm and an initial energy of 1024 kcal for the simulated annealing stage. For the DGII calculations, stereospecifically assigned β protons were designated as individual atoms; all other prochiral centers and methyl groups were replaced by pseudoatoms and an appropriate correction was applied to the upper bound distance constraint (Wüthrich et al., 1983). Prior to initiating the DGII calculations, the file containing torsion restraints (*.tors) generated by the Biosym software was edited to correct erroneous entries introduced by the program. Resulting structures were further minimized using Discover (Biosym Technologies) and a four-phase minimization schedule. During the minimization, all arbitrary prochiral assignments were reinstated and the prochiral proton assignments were allowed to float. All minimization calculations were performed in vacuo with charges ignored. The first two phases consisted of 100 steps of steepest descent minimization, followed by 500 steps of conjugate gradient minimization against the cvff91 (Biosym Technologies) potential, using only quartic nonbonded terms and a nonbonded cutoff of 5.0 Å. All distance and dihedral constraints were applied with a force constant of 160 kcal/mol and the nonbonded interactions were scaled by a factor of 0.25 during phases 1 and 2. Phases 3 and 4 were identical to 1 and 2, except that Lennard-Jones terms were incorporated, the nonbonded cutoff was increased to 12.0 Å, experimental restraint force constants were scaled down to 80 kcal/mol, nonbonded interactions were unscaled and phase 4 was allowed to iterate 1000 times. The structures were then analyzed for their consistency with the experimental restraints and were discarded if more than a total of two distance (> 0.3 Å) or dihedral violations (> 10°) were observed.

Results

Resonance assignments

Nearly complete proton assignments of all 48 amino acids were determined for a 3 mM sample dissolved in 90% H_2O/10% D_2O using sequential assignment techniques (Wüthrich, 1986) and TOCSY and NOESY spectra recorded at 15, 25 and 30 °C, as well as a double-quantum-filtered COSY spectrum recorded at 25 °C. NOESY

*A preliminary account of this work was presented at the 'Frontiers of NMR in Molecular Biology - III' Keystone Symposium, March 8–14, 1993, Taos, NM (Reily, M.D., Thanabal, V. and Adams, M.E. (1993) *J. Cell. Biochem.*, **17C**, 283 (Abstract #LXZ352)).

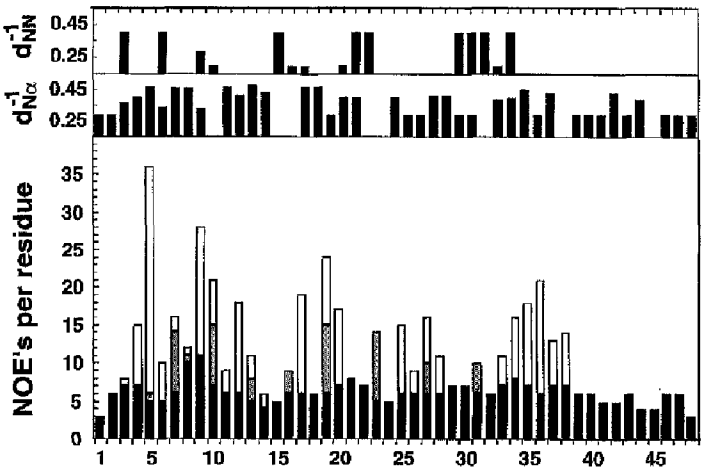

Fig. 1. Summary of NOE constraints in ω-Aga-IVB. Top: sequential backbone interactions, indicated by d^{-1}, where d is the upper bound NH-H$^{\alpha}$ or NH-NH distance constraint used in the DGII calculations. Bottom: number of NOE constraints per residue. Solid, shaded and open bars indicate sequential, medium and long-range (> i–i+4) NOEs, respectively.

spectra were recorded in H_2O and intraresidue amide-side chain cross peaks were identified by comparison to TOCSY and DQF-COSY spectra acquired under identical conditions. Sequential connectivities were observed in all cases for either H_i^{α}-NH_{i+1} or H_i^{β}-NH_{i+1}. Two prolines at positions 24 and 38 created three segments of the peptide for which uninterrupted NH-based sequential connectivities could be observed. This was facilitated by the presence of several unique dipeptides located in each of the segments, including Ile^{5}-Ala^{6}, Gly^{15}-Gly^{16}, Ile^{30}-Gly^{31}, Leu^{40}-Ile^{41} and Gly^{44}-Leu^{45}. For the two proline residues at positions 24 and 38, strong NOEs were observed between the CH$^{\alpha}$ and NH_{i+1} and between the CH$^{\alpha}$ of the preceding residue and the proline CH$^{\delta}$ resonances (in spectra recorded in D_2O), thus linking each of the segments and establishing the trans configuration for both imide bonds. A similar procedure was used to assign the resonances in a 1.5 mM sample. Samples that were freshly dissolved in D_2O allowed identification of 16 backbone amide groups that were partially shielded from exchange, 11 of which could be characterized as very slowly exchanging.

Distance and dihedral angle restraints

NOE peak intensities were initially measured by tabu-

TABLE 1
HYDROGEN BOND DONOR/ACCEPTOR STATISTICS FOR VERY SLOWLY EXCHANGING AMIDE PROTONS IN ω-Aga-IVB

Donor	Acceptor	Occurrences out of 42[a]	Average distance (Å)	Restraint	Hydrogen bonds in final structures[b]
5 HN	18 O	34	2.763	y	35
5 HN	19 O	9	2.839		0
10 HN	36 O	33	3.005		0
10 HN	8 O	39	3.693		0
10 HN	7 O	14	3.070		16
12 HN	34 O	42	2.228	y	35
12 HN	10 O	11	3.760		0
13 HN	17 O	25	3.453	y	33
19 HN	23 O	22	3.045	y	30
23 HN	19 O	29	2.833	y	25
23 HN	20 O	4	3.177		0
26 HN	35 O	42	2.151	y	35
35 HN	26 O	40	3.243	y	35
36 HN	7 O	4	3.798		0
36 HN	10 O	33	3.056	y	13
37 HN	24 O	37	3.145	y	35
37 HN	26 O	5	3.436		0
37 HN	35 O	31	2.738		0

[a] Analysis of 42 converged structures generated without hydrogen bond constraints. Excluded from the listing are intraresidue and sequential NH-acceptor atom distances and NH-acceptor atom distances > 4.0 Å.

[b] Analysis of 35 converged structures calculated with the hydrogen bond constraints indicated in column 5. Column 6 indicates the number of occurrences (out of 35 structures) of proper hydrogen bonds, as defined by InsightII (Biosym Technologies).

lating the number of contours in each assigned cross peak in selected 2D NOESY spectra. For most NOEs involving amide protons, an 80 ms NOESY spectrum recorded on a 3 mM sample in 90% H_2O at 25 °C was used; spectra recorded at 15 °C were used to evaluate the peak intensities of the few NH-H^{α} cross peaks that occurred near the water frequency at 25 °C. NOEs between non-exchangeable protons were measured from a 300 ms NOESY spectrum recorded with a 1.5 mM sample in 100% D_2O at 30 °C. These spectra were selected for analysis from a large number of spectra based on their cross-peak content and high signal-to-noise ratio. Almost all of the cross peaks observed at long mixing times (250 ms in H_2O or 300 ms in D_2O) were also observed in NOESY spectra recorded with 80 or 160 ms mixing times; the few peaks that were only seen at the longer mixing time were assigned an upper bound distance of 5 Å. In cases where cross peaks were adequately resolved, volumes were measured in arbitrary units in 80 ms (H_2O) and 300 ms (D_2O) NOESY spectra and subsequently converted into upper bound distances by comparison to a calibrated cross peak. Cross-peak volumes were calibrated by plotting V^{-6},

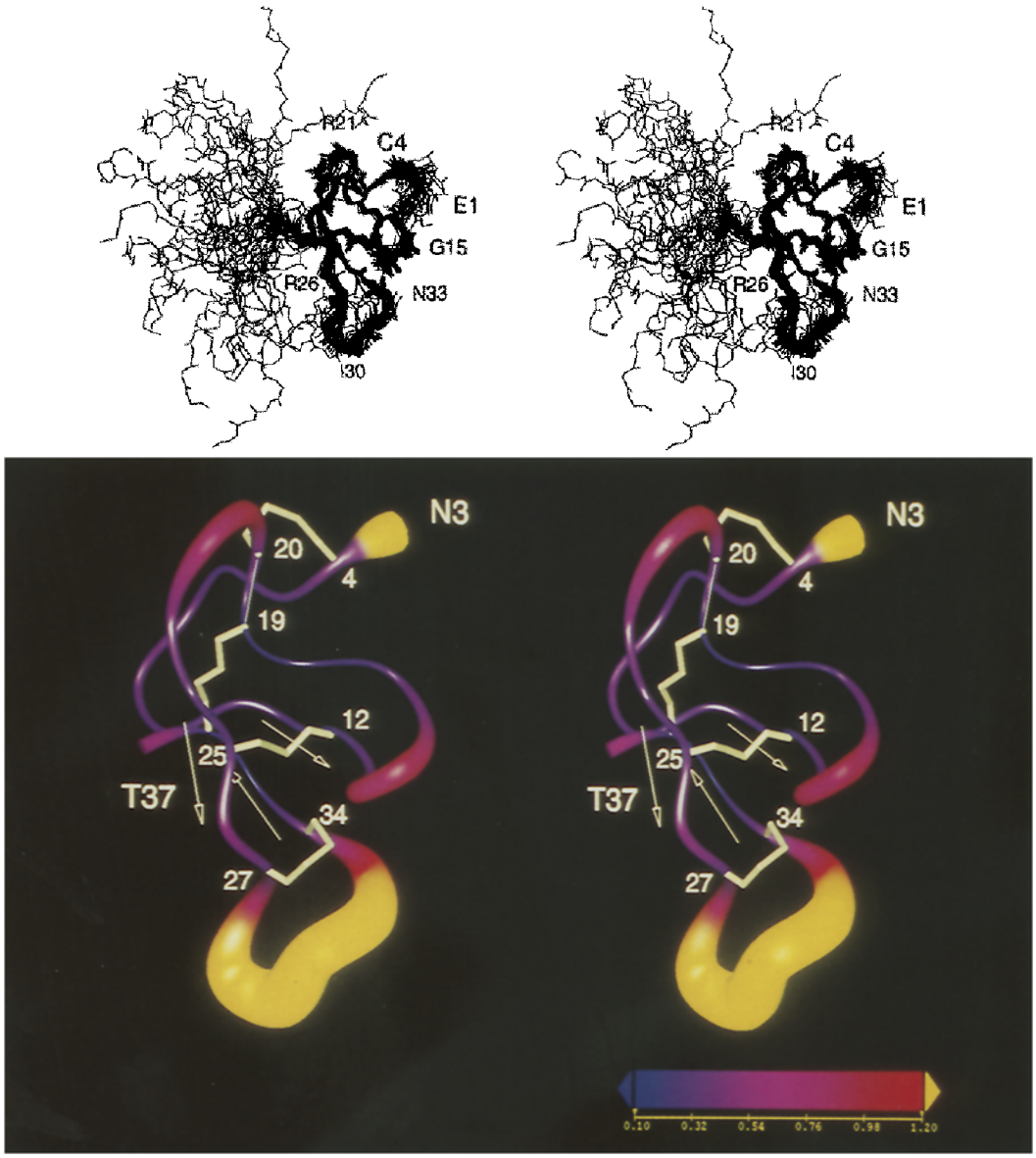

Fig 2. Thirty-five converged structures compared by superimposing backbone atoms in residues that had more than 10 long- or medium-range NOE constraints. The mean rmsd is 0.38 Å for the backbone atoms of the residues used in the superimposition, 0.63 Å for the backbone atoms of residues 4–36 and 1.18 Å for all heavy atoms in residues 4–36. Top: backbone atoms for all 48 residues. Glu^1 is oriented at the top and Ala^{48} at the bottom. Bottom: variable-width ribbon diagram for residues 3–37, showing the location of disulfides and secondary structural elements. The width of the ribbon and its color are related to the average rmsd per residue of the backbone atoms. The thinnest part of the ribbon (purple) corresponds to an rmsd of ca. 0.2 Å and the thickest part (yellow) to an rmsd of ca. 2 Å. The location of the triple-stranded β-sheet is indicated by arrows.

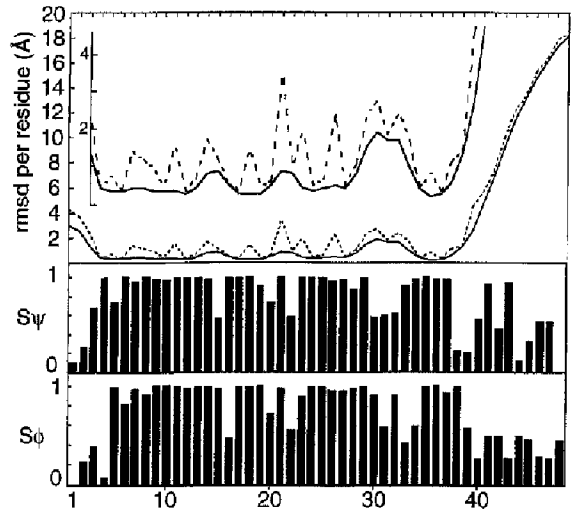

Fig. 3. Rmsd (top) and angular order parameters for ψ and ϕ (middle and bottom) of the 35 final structures.

where V is the integrated cross-peak volume corrected for 10% deuterium exchange, versus peak number for 30 well-resolved H_i^{α}-NH_{i+1} cross peaks, as previously reported (Hyberts et al., 1992). A suitable conversion factor was then determined, so that 98% of the sequential H_i^{α}-NH_{i+1} interproton distances fell within the allowed range of 2.2–3.5 Å. The most voluminous cross peak corresponded to Ile^5 H^{α}-Ala^6 NH and was assigned a distance of 2.1 Å. This conversion factor was then used to convert all of the integrated volumes to upper bound distances.

Backbone ϕ angles were constrained to a range of −90° to −10° for residues 11, 14, 17, 21, 29 and 36 and to −175° to −75° for residues 12, 13, 25, 27, 30, 32 and 35, based on $^3J_{HNH\alpha}$ values (Clore et al., 1991). Side chain χ^1 angles were constrained between 40°–80° for Cys^4 and Cys^{12}, based on the observation that $^3J_{H\alpha H\beta 2} \sim {}^3J_{H\alpha H\beta 3} \sim 4.0$ Hz for these two residues. Based on the relative size of the two $^3J_{H\alpha H\beta}$ coupling constants and the relative magnitude of the H^{α}-H^{β} and NH-H^{β} NOEs, stereospecific assignments were determined for cysteines 19, 25, 34 and 36 (Wagner et al., 1987) and χ^1 constraints were obtained for residues 19, 27 and 34 (−80° to −40°) and for residue 20 (−160° to 160°).

After generating several initial sets of structures and re-evaluating assigned NOEs (vide infra), a final restraint set was assembled consisting of 269 interproton, interresidue distances (146 sequential, 25 medium and 98 long range) from NOEs, and 13 ϕ and six χ^1 dihedral angles derived from coupling constants.

Structure calculations

An initial starting structure with extended conformation was constructed (no disulfide constraints) and 10 structures were generated using DGII. One of these structures was selected at random and the four known disulfides determined by earlier NMR analysis (Adams et al., 1993, see Scheme 1) were then defined by removing the sulfhydryl protons and creating the appropriate sulfur bonds. The resulting starting structure was subjected to unconstrained molecular dynamics at 300 K for 10 ps and then energy minimized with a steepest descent algorithm (Biosym Technologies) to an acceptably low energy. This starting structure was used in several rounds of DGII calculations and initially had relatively high error functions (Havel, 1991), due to several wrongly assigned NOEs which consistently showed up as violations in the final structures. After several iterations of DGII calculations/data correction, a majority of structures had DGII error functions <1 and displayed only small maximum distance violations (<0.3 Å). A summary of the final measured restraints used in the structure calculations is shown in Fig. 1. With these restraints, 50 structures were generated and 42 of these met the convergence criteria.

In order to assess probable hydrogen bonding in the peptide, the 42 converged structures generated with the

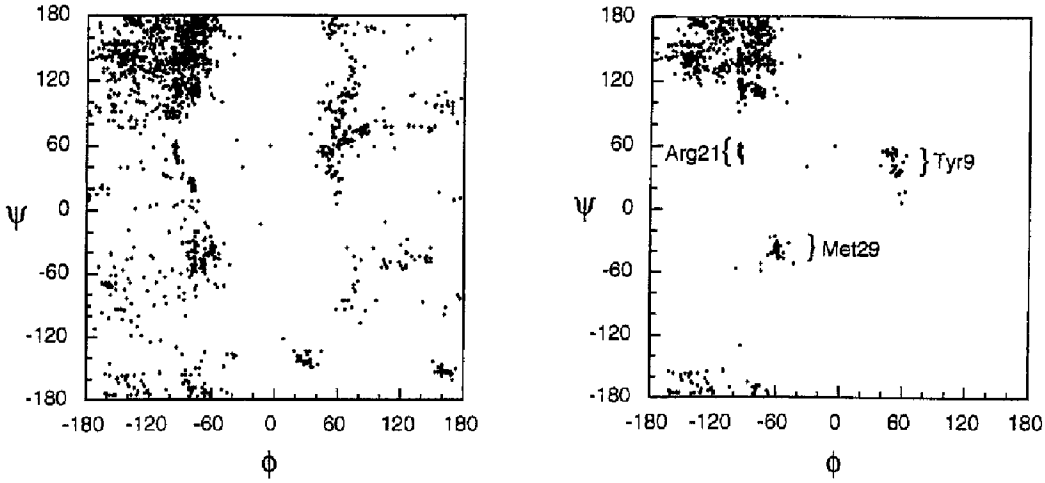

Fig. 4. Ramachandran diagram for the 35 final structures. Left: all residues for the 35 final structures. Right: only those residues for which the ϕ and ψ order parameters are ≥ 0.9.

Scheme 1. Disulfide bonds between cysteine residues in ω-Aga-IVB.

above constraints were analyzed for the proximity of hydrogen bond acceptors to very slowly exchanging amide protons. Except for Gly^{10} NH and Lys^{11} NH, all of the very slowly exchanging amide protons were within 3.5 Å of a single hydrogen bond acceptor in the majority of structures, Table 1. This analysis, combined with amide exchange and proximal NOE information, allowed distance restraints to be defined for nine hydrogen bonds. No restraint for Gly^{10} NH was used because of our inability to identify a unique acceptor atom. In order not to be too aggressive in forcing these suspected acceptor/donor pairs to adopt a favorable hydrogen bond geometry, only a generic upper bound distance of 2.35 Å between the N*H-O* atoms was added to the restraint file for each identified pair. With these incorporated, 40 new structures were generated, 35 of which met the convergence criteria; these 35 structures were used in subsequent analyses.

Discussion

Evaluation of the structures

Figure 2 shows the final 35 converged structures superimposed by the backbone atoms of residues for which there were 10 or more long- or medium-range constraints (see Fig. 1). To quantify the precision of the final structures, we have adopted some of the methods used by Wagner (Hyberts et al., 1992). The protocol involves analysis of variability among the structures based on rms differences in coordinates and backbone angular order parameters. The rms differences per residue, <rmsd>, were calculated from the average coordinates and regional rmsd values are the average of <rmsd> for a given set of atoms over the residues that make up the region (e.g., $<rmsd>_{10-20bb}$ and $<rmsd>_{10-20hv}$ refer to the average backbone and heavy atom rmsd values for residues 10 through 20, respectively). The <rmsd> and angular order parameters calculated for the final 35 structures are shown in Fig. 3. The final structures are quite similar between the first and last cysteine residue, with $<rmsd>_{4-36bb}$ = 0.63 Å and $<rmsd>_{4-36hv}$ = 1.18 Å. Within the cystine-rich portion of the molecule, regions of higher rmsd correspond to loops, some of which are better defined than others (vide infra). The N-terminal residues (1–3) and C-terminal residues (37–48) lie outside the cystine-rich region and display

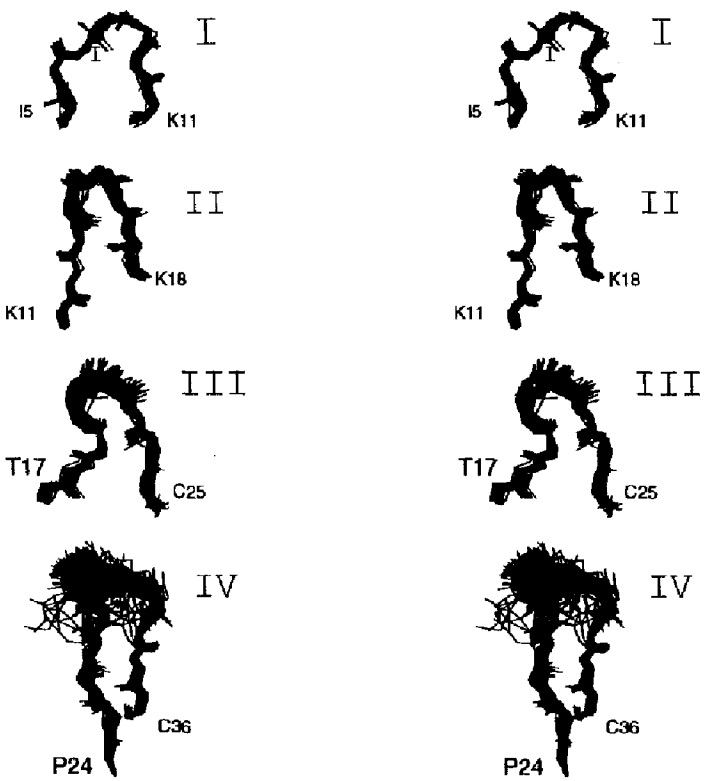

Fig 5. Stereoviews (relaxed) of the loop regions in ω-Aga-IVB. The backbone atoms in residues that had more than 10 long- or medium-range NOE constraints were superimposed in the 35 converged full structures.

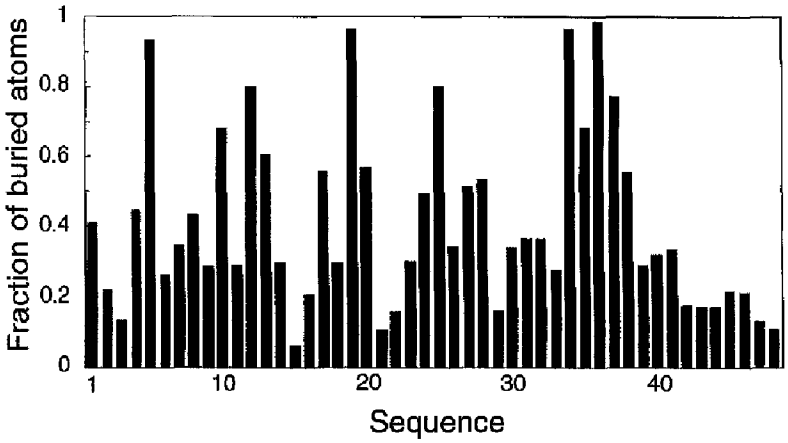

Fig. 6. Solvent-inaccessible residues in ω-Aga-IVB. The heights of the bars indicate the fraction of atoms per residue that do not contact a 1.4 Å spherical probe in Connolly calculations on nine of the final structures (see text).

much larger rmsd values. In all cases, higher rmsd values correlated well with a smaller number of restraints per residue (Fig. 1), coupling constants that tend to be in the motionally averaged range of 7 Hz, and chemical shifts that are close to 'random coil' values (Williamson, 1990).

Plotting the ϕ versus ψ values for all of the 35 final structures allows evaluation of the quality of the final structures with respect to allowed regions in a Ramachandran diagram, Fig. 4. Twenty residues, all located in the cystine-rich region of the molecule, have S_ϕ and $S_\psi \geq 0.9$. By plotting ϕ versus ψ for these 20 residues it becomes clear that nearly all of the points that appear in disallowed regions are due to residues in the peptide that have a high degree of disorder. Most of the 19 well-defined residues lie within the β-region of the Ramachandran map, exceptions being Tyr^9, Arg^{21} and Met^{29}. The average ϕ,ψ values for Tyr^9, Arg^{21} and Met^{29} are 40°,55°, −90°,50° and −59°,−43°, respectively. In the case of Tyr^9, which occurs in the α_L/γ_L region of the Ramachandran plot, the side chain and backbone are well defined due to the large number of NOEs observed. Interestingly, early calculations in which we included a torsion constraint of −10° to −90°, consistent with the observed coupling constant of 5.9 Hz, resulted in a large number of errors in NOEs involving Tyr^9 and nearby residues. Removal of this single torsional constraint significantly reduced the number and size of NOE violations, but resulted in structures that invariably had positive ϕ values for Tyr^9. A positive ϕ is consistent with the observations of a very strong intraresidue NH-H^α NOE and a relatively small $^3J_{NH,H^\alpha}$ of 5.9 Hz for Tyr^9. This coupling constant is within the range observed for residues with similar positive ϕ values in other proteins (Ludvigsen and Poulsen, 1992) and Tyr^9 has a positive ϕ in the previously reported structure (Yu et al., 1993). The ϕ,ψ space occupied by Arg^{21} is consistent with its apparent occurrence at the i+1 position in an

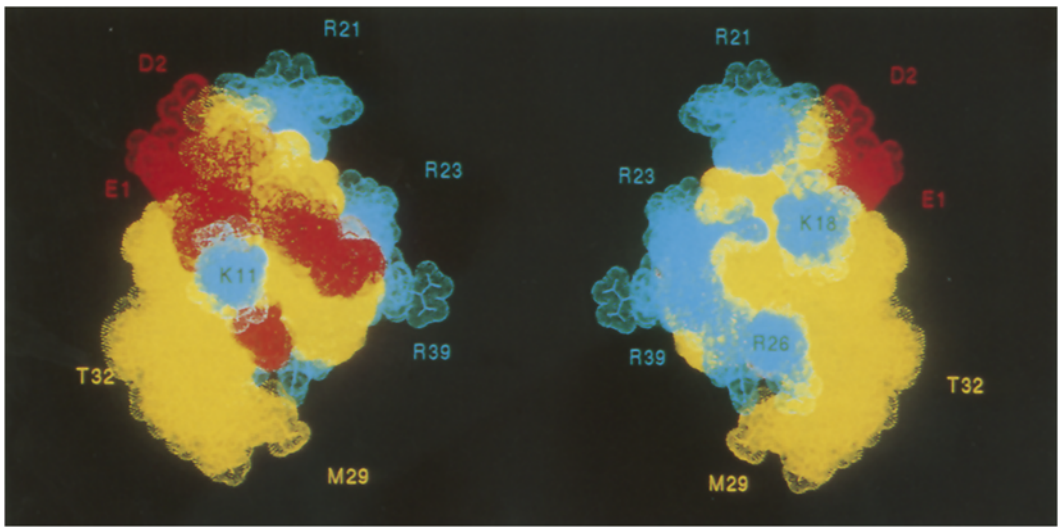

Fig. 7. Views of the charge distribution in the three-dimensional structure of ω-Aga-IVB. The figure contains nine superimposed van der Waals surface models, showing the location of the negatively (red) and positively (blue) charged side chains in ω-Aga-IVB.

inverse γ-turn (vide infra). Met[29] occurs in the α_R region of ϕ,ψ space. There are no long- or medium-range NOEs involving Met[29] and it occurs in a region of the peptide characterized by relatively high rmsd values (Fig. 3), yet the corresponding backbone angular order parameters are high. The relatively small $^3J_{NH,H^\alpha}$ of 5.3 Hz supported the assignment of a torsional constraint of −10° to −90° in the DGII and energy minimization calculations. This constraint, combined with a strong Met[29] NH-Ile[30] NH NOE, is probably the reason for the observed ϕ,ψ values. This structural assignment is also consistent with the observed medium-intensity intraresidue NH-H^α NOE seen for Met[29], which would be expected to be more intense if the residue were highly flexible. Despite these points, because of the apparent flexibility in this region of the peptide, it is difficult to be certain whether the high degree of order in the Met[29] ϕ and ψ angles is real or an artifact. Even if it is real, however, it is a localized order and its actual three-dimensional coordinates with respect to the rest of the structure are uncertain, see Figs. 3 and 4.

Beta sheet

Preliminary analysis of the nonsequential long-range NOEs confirmed previous NMR reports (Adams et al., 1993; Yu et al., 1993) of a three-stranded antiparallel β-sheet comprising residues 10–12, 25–27 and 34–36, see Fig. 2. This β-sheet has a +2x, −1 (Richardson, 1981) topology which is, interestingly, the same classification as the β-sheet recently reported for another peptide toxin, ω-conotoxin GVIA (Davis et al., 1993), which is a selective antagonist of N-type calcium channels. This secondary structure was characterized by several H^α-H^α, H^α-NH and NH-NH interstrand NOEs, as well as by the fact that most of the backbone amide protons exchanged very slowly, the latter being consistent with interstrand hydrogen bonding. The residues that participate in the β-sheet are well defined, with $\langle rmsd \rangle_{10-12,25-27,34-36}$ = 0.36 Å and 0.85 Å for the backbone and heavy atoms, respectively. The coupling constants measured for some of these residues are smaller than expected for canonical ϕ angles found in β-sheets, suggesting an irregular sheet structure. This is not entirely unexpected, since a large number of cystines is present in this region of the peptide, including a disulfide bond across two strands of the β-sheet between Cys[27] and Cys[34]. This disulfide may disrupt the sheet leading into the β-bend, and no evidence for interstrand NOEs or slowly exchanging NHs consistent with a β-sheet are observed for residues 28, 29, 32 or 33.

Turns

Several turns in the peptide were initially identified by the standard criteria that C^α_i is less than 7 Å from C^α_{i+3} and that the residues at positions i+1 and i+2 are not helical (Lewis et al., 1973). Analysis of the ensemble of final structures resulted in six i–i+3 pairs that were < 7.0 Å apart in all 35 structures: 7–10, 13–16, 19–22, 20–23, 28–31 and 31–34. The superimposed backbone atoms for each of the regions that contain these residues are shown in Fig. 5.

The residues that comprise the first turn (loop I), Glu[7]-Asp[8]-Tyr[9]-Gly[10], are well defined, both in terms of average backbone rmsd ($\langle rmsd \rangle_{7-10bb}$ = 0.38 Å) and angular order parameters, see Fig. 3. The average ϕ,ψ angles for Asp[8] and Tyr[9] are −86°,129° and 55°,40°, respectively and are therefore classified as $\beta_P\gamma_L$ type using Ramachandran nomenclature (Wilmot and Thornton, 1990); this is equivalent to a distorted type II β-turn. A strong NOE was observed between H^α_{i+1} and NH_{i+2}, but not between NH_{i+1} and NH_{i+2}, consistent with a $\beta_P\gamma_L$ type turn (Wüthrich et al., 1983). Gly[10] NH exchanges very slowly and may be involved in a hydrogen bond to the Glu[7] carbonyl oxygen (vide infra).

Loop II consists of Thr[13]-Trp[14]-Gly[15]-Gly[16] and also evaluates as a $\beta_P\gamma_L$ type turn. The average ϕ,ψ angles for Trp[14] and Gly[15] are −90°,106° and 93°,45°, respectively. These residues are also well ordered, although somewhat less than in loop I ($\langle rmsd \rangle_{13-16bb}$ = 0.67 Å). The major locus of disorder appears to be the backbone dihedral angles between Gly[15] and Gly[16]. As with loop I, we observed i+1–i+2 NOEs and Gly[16] NH exchanges slowly, consistent with the expected i+3–i hydrogen bond.

A third turn which reverses the peptide backbone between residues 19 and 23, loop III, is well ordered ($\langle rmsd \rangle_{19-23bb}$ = 0.57 Å), and may be an inverse γ-turn. In this turn, there are two spatially close i–i+3 pairs, 19–22 and 20–23. A large number of NOEs and two hydrogen bonds (Table 1) between Cys[19] and Arg[23] essentially hold these two residues in register across from each other, allowing only three amino acids, Cys[20], Arg[21] and Gly[22], to form the strand-reversing turn. Furthermore, the average ϕ,ψ values for Arg[21] are −91°,50°, within the range expected for the i+1 residue in an inverse γ-turn (Milner-White, 1990).

The residues between the disulfide bond at positions 27 and 34 (loop IV) reverse the direction of the backbone between two strands in the β-sheet. This turn is also characterized by two close i–i+3 contacts, 28–31 and 31–34; however, these residues are much less ordered than loops I–III ($\langle rmsd \rangle_{28-34bb}$ = 1.31 Å). In a canonical strand-turn-strand antiparallel β-sheet, residues 28 and 33 would also be fully involved in the β-sheet structure, and 29–32 would comprise the β-turn. Thr[32] NH exchanges slowly and a hydrogen bond formed with the Met[29] carbonyl oxygen would be consistent with such a β-turn. However, several lines of evidence argue against a typical strand-turn-strand structure. First, Asn[33] has a relatively small $^3J_{H^NH^\alpha}$ of 7.4 Hz, smaller than expected for a β-sheet residue (the $^3J_{H^NH^\alpha}$ for Ser[28] could not be measured unambiguously). Second, a strong NOE is observed between Cys[34] NH and Asn[33] NH; this is inconsistent with the expected distance

of ca. 4 Å between these atoms in a canonical β-sheet structure. Third, the ϕ angles for residues 30–34 and the ψ angles for residues 30–32 have low order parameters (see Fig. 3), consistent with the high rmsd in this region. Fourth, only two of the 35 final structures had Met^{29} C^{α}-Thr^{32} C^{α} distances < 7.0 Å. Fifth, no interresidue NH-NH NOEs are observed between residues 28 and 33, as would be expected in a normal β-sheet structure. Finally, the Ser^{28} NH undergoes rapid NH-ND exchange. These points are all accounted for if significant conformational flexibility is assumed in loop IV.

Core residues

The disulfide bonds constrain the cystine-rich region of ω-Aga-IVB in three-dimensional space. As expected for such a small protein, most of the residues are solvent-exposed. To identify residues that were solvent-shielded, a Connolly surface (Connolly, 1983) was calculated using a spherical probe, 1.4 Å in diameter, for each of the nine structures that had the lowest rmsd from the average. The fraction of buried atoms per residue was calculated by summing the number of atoms that had no contact with the probe in each residue and dividing by the number of atoms in that residue. This number was then averaged over the nine structures and resulted in the histogram shown in Fig. 6. A majority of the solvent-shielded atoms arose from cysteines 12, 19, 25, 34 and 36. In addition, parts of Ile^{5} and Gly^{10} were close to the side chains of these cysteines and were well inside the calculated Connolly surface. Each of the seven residues identified in this way shows a large number of long- and medium-range NOEs, see Fig. 1. Also, each of the 11 slowly exchanging NH protons is in close proximity to one or more of these seven residues.

Hydrogen bonding network

To assess the hydrogen bonds present in the final 35 structures we looked for acceptor/donor pairs that were within 2.4 Å of each other and had a good geometry (N-H-O angle of ≥ 120°). Most of the NH/O pairs for which we included a generic distance restraint (vide supra) showed good hydrogen bond geometry, Table 1. These hydrogen bonds adequately explain 9 of the 11 observed very slowly exchanging NH groups, the exceptions being the backbone amides of Gly^{10} and Lys^{11}. The only reasonable interaction for Gly^{10} NH is with the Glu^{7} O, and a hydrogen bond is seen here in 16 of the 35 final structures. Also, the average distance between these two atoms across the entire ensemble is 3.0 Å. Solvent-accessible surface calculations (vide supra) indicate that Lys^{11} NH is located near the surface of the molecule and is solvent-exposed, therefore some sort of hydrogen bonding must be present to explain its very slow exchange. Excluding potential donor atoms within Lys^{11} itself and in adjacent residues, the only potential donor atoms seen consistently across the ensemble of final structures (within 4.5 Å) for Lys^{11} NH are the side-chain oxygens of Glu^{7}. In 13 of the 35 final structures, one of the side-chain oxygen atoms is close to the Lys^{11} NH, with an average H-O distance of 3.8 Å in the 13 structures. Glu^{7} and Gly^{10} comprise the i and i+4 residues of loop I and although there are no NOEs between Glu^{7} and Lys^{11}, the two residues are reasonably close to each other in the calculated structures. In addition to the loosely restrained hydrogen bonds included in the calculations, hydrogen bonds were also observed between Gly^{10} NH and Glu^{7} O in 16 structures, between Glu^{7} NH and Ile^{5} O in 20 structures, between Gly^{22} NH and Cys^{19} O in 23 structures and between Cys^{20} NH and Ile^{5} O in 19 structures. The latter three NHs exchange rapidly with D_2O and are observed to be solvent-exposed in a majority of structures that were subjected to solvent accessibility calculations.

The N- and C-termini

The tail regions and particularly the C-terminus of ω-Aga-IVB are very poorly defined (Figs. 3 and 4), with no NOEs suggesting an interaction with the cystine-rich portion of the molecule. There is, however, some evidence for transient structure within the tail region, namely some residues have reduced amide proton temperature coefficients and show small deviations from 'random coil' chemical shifts (data not shown). It has been suggested that the C-terminal tail of the peptide acts to occlude the conductance pathway of the channel or, alternatively, acts as a hydrophobic anchor that deposits the toxin into the lipid bilayer (Yu et al., 1993). The specific roles of the termini await pharmacological evaluations of mutated toxins related to ω-Aga-IVB.

Charged residues

ω-Aga-IVB displays an interesting array of positively charged residues, clustered on one face of the molecule. Several of these cationic side chains are common between ω-Aga-IVB and ω-Aga-IVA (Adams et al., 1993), suggesting that these residues are likely to be involved in binding to the negatively charged extracellular surface of the calcium channel. Figure 7 shows a surface rendering for nine of the final structures. Three of the arginine residues (at positions 21, 23 and 39) are conserved between ω-Aga-IVB and ω-Aga-IVA and, as is common for surface-mounted arginines, are ill defined in the ensemble of structures, with $\langle rmsd \rangle_{hv}$ values of 3.49, 1.90 and 4.59 Å, respectively. Nonetheless, these side chains clearly reside on one surface of the molecule. If these residues are important for binding and selectivity, they are likely to adopt a more rigid conformation upon binding to the calcium channel. Unfortunately, little can be concluded about the bound conformation of such side chains from a solution structure of the toxin alone. Despite the large number of possible orientations of the side chains of these

TABLE 2
INTERACTIONS LEADING TO STEREOSPECIFIC ASSIGNMENTS FOR FOUR CYSTEINE RESIDUES IN ω-Aga-IVB[a]

Residue	$^3J_{H^\alpha H^\beta}$	$^3J_{H^\alpha H^{\beta'}}$	$d_{H^\alpha H^\beta}$	$d_{H^\alpha H^{\beta'}}$	d_{NHH^β}	$d_{NHH^{\beta'}}$	Stereospecific assignment[b] $H^{\beta 2}$	$H^{\beta 3}$
Cys^{19}	−	+	+	−	−	+	$H^{\beta'}$	H^{β}
Cys^{25}	+	−	−	+	+	−	H^{β}	$H^{\beta'}$
Cys^{34}	−	+	+	−	−	+	$H^{\beta'}$	H^{β}
Cys^{36}	+	−	−	+	+	−	H^{β}	$H^{\beta'}$

[a] This analysis is based on observed intraresidue J couplings and NOE intensities as previously described (Wagner et al., 1987). A plus sign indicates a strong interaction, either a large coupling constant or an intense NOE; a minus sign has the opposite meaning.
[b] For cysteine, IUPAC nomenclature equates H^{32} and $H^{\beta 3}$ with *S* and *R* prochirality, respectively. Upfield and downfield H^β protons are designated H^β and $H^{\beta'}$, respectively.

three residues, by measuring the distance between extrema in the allowed space for the three arginines in Fig. 7, an upper limit estimate of the size of this possible site of ionic interaction with the channel of approximately 20 × 20 Å can be made. This is similar in size to the recently described hypothesized surface contact area between charybdotoxin and the K^+ Shaker channel (Goldstein et al., 1994). Additional charged groups are indicated in the spacefilling model shown in Fig. 7. Many of these residues are not conserved in ω-Aga-IVA and indeed, particularly in the N-terminus, some are oppositely charged between the two peptides. Even so, these relatively significant differences do not result in great differences in the binding affinity for the P-type calcium channel (2 nM for ω-Aga-IVA and 3 nM for ω-Aga-IVB), but may influence the slower kinetics of channel block and unblock observed for ω-Aga-IVB (Adams et al., 1993).

Comparison with previous structures

This work has allowed us to greatly improve the resolution of the preliminary structure of ω-Aga-IVB reported earlier (Adams et al., 1993). With a few exceptions, the structure reported here is in good agreement with the work reported by Yu et al. (1993) describing the solution structure of ω-Aga-IVB at pH 4.0. In the paper by Yu et al., the reported average rmsd for the backbone atoms, excluding the N- and C-termini, was 1.17 Å compared with the 0.63 Å we observe. This is due, in part, to the larger number of long- and medium-range NOEs used in this study (123 vs. 107 in the Yu paper) and the calibration methods used here. Yu et al. concluded that the peptide segment from Thr^{13} to Pro^{24} does not adopt a regular secondary structure, although the present work suggests that this region of the peptide contains a well-defined $\beta_P\gamma_L$-turn and possibly an inverse γ-turn (vide supra). Examination of the average minimized structure from the previous work (PDB code: 1omb) reveals the presence of two turns in this region, the first of which corresponds with loop II (residues 13–16) and has backbone angles for the i+1 and i+2 residues similar to those reported here. The second turn occurs at the same location as loop III, but the backbone angles are dissimilar for the residues that make up the turn. Another notable difference is the number of slowly exchanging NH protons, 14 in this work versus only three in the previous report. This is possibly due to the higher pH and/or the presence of buffers, or to the higher temperature used in the previous study.

The major discrepancies between the assignments reported by Yu et al. and the present work involve the chemical shifts of the Arg^{23} H^δ protons and the stereospecific assignment of the Cys^{19}, Cys^{25} and Cys^{36} H^β protons. Yu et al. report a single chemical shift of 2.78 ppm for Arg^{23} H^δ, whereas in this study Arg^{23} displays two H^δ resonances that are separated by 0.33 ppm. The average chemical shift of the two H^δ protons is close to the value reported in the previous study, and therefore it is possible that the Arg^{23} side chain is somewhat less mobile under the conditions used in this study. Indeed, Arg^{23} is the most highly ordered of all the arginine residues, with $\langle rmsd \rangle_{23hv}$ = 1.90 Å compared with 3.49, 2.44 and 4.59 Å for arginines 21, 26 and 39, respectively. Our stereospecific assignments for four pairs of cysteine H^β protons was determined by analysis of intraresidue NOE intensities and scalar coupling constants between NH, H^α and H^β protons, as previously described (Wagner et al., 1987). In the four cases where we were able to make stereospecific assignments, the H^β protons were baseline separated and the intraresidue scalar and dipolar cross peaks were sufficiently resolved to be accurately integrated. Table 2 summarizes the intraresidue interactions we observed. For the H^β protons of the three cysteines, where discrepancies exist between this work and that of Yu et al., 35 interresidue NOEs have been assigned. Since many of these have different upper bound constraints between a common atom and the two H^β protons, one would expect the differences in stereospecific assignments to have an impact on the final structures; this may also be reflected in the discrepancies seen between the rmsd values of the final structure.

Conclusions

The peptide described in this report, ω-Aga-IVB, is the first selective P-type calcium channel antagonist whose

three-dimensional structure has been elucidated. The 3D structure of this peptide consists of a well-defined cystine-rich region comprising an irregular triple-stranded β-sheet, four loop regions, and essentially disordered N- and C-termini. The cystine-rich region contains all of the amino acids which occur within the β-sheet and loops, as well as all of the solvent-inaccessible side chains and amide protons. Interestingly, apparently neither of the prolines are involved in turns in the peptide; Pro^{24} lies between loops III and IV, in a somewhat extended region near the end of a strand of the β-sheet. Pro^{38} lies outside the cystine-rich region and its structure is not well defined. The topology of several of the basic amino acids, which may be important in the binding of the peptide to the calcium channel, are clustered on one face of the molecule.

Comparison of this structure with that of the selective N-type channel toxin, ω-conotoxin-GVIA, reveals a similar overall fold but also significant structural differences which may be determinants for selectivity. First, both peptides contain a loop which reverses the direction of the peptide backbone between two strands of a β-sheet. This loop, however, is eight amino acids longer in ω-Aga-IVB than in GVIA. Since the overall conformation of the peptides is similar, it is reasonable to assume that they interact with the calcium channel in a similar way and therefore, the extension of this loop may directly reflect a structural difference between the N-type and P-type calcium channels. Second, ω-Aga-IVB has 10 extra C-terminal amino acids; these form a disordered hydrophobic tail which is not associated with the constrained interior region of the peptide. This observation suggests an additional (hydrophobic) interaction between ω-Aga-IVB and the P-type channel or the surrounding membrane that is absent in the N-type channel complex.

The surfaces presented by these peptides hold promise for the rational design of biologically active, truncated peptides based not on the primary sequence of the toxin but on its molecular topology. An additional benefit of studying these peptides is that current methods available for atomic resolution structural analysis of biomolecules are not amenable to the study of ion channels directly; the latter exist as membrane-bound conglomerates of thousands of amino acids whose structure is dependent on the presence of a lipid bilayer. Thus, understanding how the shape of rigid peptide ligands determines their interaction with the channel provides both an indirect look at the structure of the ion channel itself (Stampe et al., 1994) and answers important questions regarding the molecular basis for binding and selectivity. As the database of these structures accumulates, we will be better able to answer probing questions about specificity and mode of action in these compounds, with the potential for design of new pharmacological tools and neuroprotective agents.

The coordinates of the 35 final structures will be deposited in the Brookhaven Database, along with the constraints used in the DGII/Discover calculations.

Acknowledgements

Thanks to Mr. Chris Ingalls for writing the computer programs to calculate the rmsd and the order parameters and to analyze the hydrogen bonding. Thanks also to Dr. Lakshmi Narasimhan and Ms. Diana Omecinsky for helpful discussions.

References

Adams, M.E., Mintz, I., Reily, M.D., Thanabal, V. and Bean, B. (1993) *Mol. Pharmacol.*, **44**, 681–688.

Bax, A. and Davis, D.G. (1985) *J. Magn. Reson.*, **65**, 355–360.

Braunschweiler, L. and Ernst, R.R. (1983) *J. Magn. Reson.*, **53**, 521–528.

Clore, G.M., Wingfield, P.T. and Gronenborn, A.M. (1991) *Biochemistry*, **30**, 2315–2323.

Connolly, M.L. (1983) *J. Appl. Crystallogr.*, **16**, 548–558.

Davis, J.H., Bradley, E.K., Miljanich, G., Nadasdi, L., Ramachandran, J. and Basus, V. (1993) *Biochemistry*, **32**, 7396–7405.

Goldstein, S.A.N., Pheasant, D.J. and Miller, C. (1994) *Neuron*, **12**, 1377–1388.

Havel, T.F. (1991) *Prog. Biophys. Mol. Biol.*, **56**, 43–78.

Hyberts, S.G., Goldberg, M.S., Havel, T.F. and Wagner, G. (1992) *Protein Sci.*, **7**, 736–751.

Kumar, A., Ernst, R.R. and Wüthrich, K. (1980) *Biochem. Biophys. Res. Commun.*, **95**, 1–6.

Lewis, P.N., Momany, F.A. and Scheraga, H.A. (1973) *Biochim. Biophys. Acta*, **303**, 211–229.

Ludvigsen, S. and Poulsen, F.M. (1992) *J. Biomol. NMR*, **2**, 227–233.

Marion, D. and Wüthrich, K. (1983) *Biochem. Biophys. Res. Commun.*, **113**, 967–974.

Milner-White, E.J. (1990) *J. Mol. Biol.*, **216**, 385–397.

Mintz, E.M., Venema, Y.J., Swiderek, K.M., Lee, T.D., Bean, B.P. and Adams, M.E. (1992) *Nature*, **355**, 827–829.

Olivera, B.M., Miljanich, G., Ramachandran, J. and Adams, M.E. (1994) *Annu. Rev. Biochem.*, **63**, 823–867.

Reily, M.D., Holub, K.E., Gray, W.R., Norris, T.M. and Adams, M.E. (1994) *Nature Struct. Biol.*, **1**, 853–856.

Richardson, J.S. (1981) *Adv. Protein Chem.*, **34**, 167–339.

Sevilla, P., Bruix, M., Sanatoro, J., Gago, F., Garcia, A.G. and Rico, M. (1993) *Biochem. Biophys. Res. Commun.*, **192**, 1238–1244.

Skinner, W.S., Adams, M.E., Quistad, G.B., Kataoka, H., Cesarin, B.J., Enderlin, F.E. and Schooley, D.A. (1989) *J. Biol. Chem.*, **264**, 2150–2155.

Stampe, P., Kolmakovapartensky, L. and Miller, C. (1994) *Biochemistry*, **33**, 443–450.

Valentino, K., Newcomb, R., Gadbois, T., Singh, T., Bowersox, S., Bitner, S., Justice, A., Yamashiro, D., Hoffman, B.B., Ciaranello, R., Miljanich, G. and Ramachandran, J. (1993) *Proc. Natl. Acad. Sci. USA*, **90**, 7894–7897.

Wagner, G., Braun, W., Havel, T.F., Schaumann, T., Gō, N. and Wüthrich, K. (1987) *J. Mol. Biol.*, **196**, 611–639.

Williamson, M.P. (1990) *Biopolymers*, **29**, 1423–1431.

Wilmot, C.M. and Thornton, J.M. (1990) *Protein Eng.*, **3**, 479–493.

Wüthrich, K. (1986) *NMR of Proteins and Nucleic Acids*, Wiley, New York, NY.

Wüthrich, K., Billeter, M. and Braun, W. (1983) *J. Mol. Biol.*, **169**, 949–961.

Yu, H., Rosen, M.K., Saccomano, N.A., Phillips, D., Volkmann, R.A. and Schreiber, S.L. (1993) *Biochemistry*, **32**, 13123–13129.